Permeation Properties of Inward-Rectifier Potassium Channels and Their Molecular Determinants

Han Choe,* Henry Sackin,‡ and Lawrence G. Palmer*

From the *Department of Physiology and Biophysics, Weill Medical College of Cornell University, New York, New York 10021; and the ‡Department of Physiology and Biophysics, The Chicago Medical School, North Chicago, Illinois 60064

abstract The structural domains contributing to ion permeation and selectivity in K channels were examined in inward-rectifier K^+ channels ROMK2 (Kir1.1b), IRK1 (Kir2.1), and their chimeras using heterologous expression in *Xenopus* oocytes. Patch-clamp recordings of single channels were obtained in the cell-attached mode with different permeant cations in the pipette. For inward K^+ conduction, replacing the extracellular loop of ROMK2 with that of IRK1 increased single-channel conductance by 25 pS (from 39 to 63 pS), whereas replacing the COOH terminus of ROMK2 with that of IRK1 decreased conductance by 16 pS (from 39 to 22 pS). These effects were additive and independent of the origin of the NH_2 terminus or transmembrane domains, suggesting that the two domains form two resistors in series. The larger conductance of the extracellular loop of IRK1 was attributable to a single amino acid difference (Thr versus Val) at the 3P position, three residues in front of the GYG motif. Permeability sequences for the conducted ions were similar for the two channels: $Tl^+ > K^+ > Rb^+ > NH_4^+$. The ion selectivity sequence for ROMK2 based on conductance ratios was NH_4^+ (1.6) > K^+ (1) > Tl^+ (0.5) > Rb^+ (0.4). For IRK1, the sequence was K^+ (1) > Tl^+ (0.8) > NH_4^+ (0.6) >> Rb^+ (0.1). The difference in the NH_4^+ / K^+ conductance (1.6) and permeability (0.09) ratios can be explained if NH_4^+ binds with lower affinity than K^+ to sites within the pore. The relatively low conductances of NH_4^+ and Rb^+ through IRK1 were again attributable to the 3P position within the P region. Site-directed mutagenesis showed that the IRK1 selectivity pattern required either Thr or Ser at this position. In contrast, the COOH-terminal domain conferred the relatively high Tl^+ conductance in IRK1. We propose that the P-region and the COOH terminus contribute independently to the conductance and selectivity properties of the pore.

key words: ROMK • IRK • NH_4^+ • Tl^+ • Rb^+ • selectivity

INTRODUCTION

Permeation is the defining property of an ion channel and has been a subject of intensive studies (Hille, 1992). It is now well established that ions move through the pore by an electrodiffusive mechanism whose molecular determinants are beginning to be understood. One of the fundamental questions concerning permeation is how an ion channel can have a simultaneous high conductance and high selectivity since selectivity implies strong interactions between the ions and the pore (Latorre and Miller, 1983).

Almost all K^+ channels are >100-fold times as permeable to K^+ as to Na^+ or Li^+ (Hille, 1992). This high selectivity can be accounted for by the close-fit hypothesis based on the size of Na^+ (1.90 Å) and K^+ (2.66 Å) (Mullins, 1959; Bezanilla and Armstrong, 1972; Hille, 1973). The crystal structure of KcsA channel supports this hypothesis, and furthermore reveals that the K^+ ion is coordinated by backbone carbonyl oxygens in the selectivity filter (Doyle et al., 1998).

Other monovalent cations, NH_4^+, Rb^+, and Tl^+, have sizes (3.00, 2.96, and 2.80 Å, respectively; Hille, 1973) similar to that of K^+, and indeed many K^+ channels conduct those ions with different rates. The selectivity among these ions is thought to occur by different affinities at binding sites within the pore and different rates of translocation to and from these sites.

The inward-rectifier K^+ channel (Kir)[1] is a tetramer (Glowatzki et al., 1995; Yang et al., 1995b), where each subunit has two transmembrane domains: M1 and M2 (for reviews, see Jan and Jan, 1997; Nichols and Lopatin, 1997). Both NH_2 and COOH termini are located in the cytoplasm, and the extracellular loop (ECL) contains a P region that forms a selectivity filter. Sequence similarity suggests that the Kir channel is homologous to the core (S5, S6, and H5) structure of voltage-gated K^+ channels (Kv).

There is evidence that both the COOH-terminus and the H5 (pore) region of the channel are important for determining the K^+ conductance of the Kir and Kv families (Lopez et al., 1994; Taglialatela et al., 1994;

Portions of this work were previously published in abstract form (Choe, H., H. Sackin, and L.G. Palmer. 1999. *Biophys. J.* 76:A78) and in a dissertation in partial fulfillment of requirements of a Ph.D. degree (Choe, 1999).

Address correspondence to Lawrence G. Palmer, Department of Physiology and Biophysics, Cornell University Medical College, 1300 York Avenue, New York, NY 10021. Fax: 212-746-8690; E-mail: lgpalm@mail.med.cornell.edu

[1]*Abbreviations used in this paper:* ECL, extracellular loop; Kir, inward-rectifier K^+ channel.

Zhou et al., 1996; Choe et al., 1999). It is not known whether these two regions form independent barriers to ion movement or whether the structure of one could modulate the properties of the other.

Previously, we have described the gating mechanism of ROMK2 (Kir1.1b) (Choe et al., 1998) and the structural determinants of the Kir channel gating (Choe et al., 1999). Here we report the permeation properties of Kir channels and explore the molecular determinants of channel conductance and permeation. Guided by the finding that two members of the Kir channel family, ROMK2 and IRK1, have different conductances and different selectivities for the cations (K^+, NH_4^+, Rb^+, and Tl^+ ions), we used chimeras of these two channels to investigate which parts of the inward rectifier structure are responsible for differences in ion permeation.

METHODS

Construction of Chimeras

The construction of the chimeras between ROMK2 (Zhou et al., 1994) and IRK1 (Kubo et al., 1993) has been previously described (Choe et al., 1999). The designs of the chimeras were based on division of the ROMK and IRK subunit structures into seven homologous and interchangeable regions. These are indicated in Fig. 1 as: (a) the N-terminus, (b) the M1 transmembrane segment, (c) the MP region, (d) the highly conserved pore (P) domain, (e) the PM segment, (f) the M2 transmembrane segment, and (g) the COOH terminus. The pore alpha-helix includes both the latter part of the MP segment and the first part of the P region. The amino acids of the seven segments are defined in Figure 4 of Choe et al. (1999).

Primers were synthesized by Operon Technologies, Inc. (Alameda, CA). Nucleotide sequences between two restriction enzyme sites were checked using an ABI 377 automated DNA sequencer at The Rockefeller University DNA Technology Center (New York, NY), or an ABI 377XL automated DNA sequencer at The Cornell University Bioresource Center (Ithaca, NY).

Expression of Channels

Plasmids were linearized with NotI restriction enzyme and transcribed in vitro with T7 RNA polymerase in the presence of the GpppG cap using mMESSAGE mMACHINE kit (Ambion, Inc.). cRNA pellet was dissolved in Ultraspec water containing DEPC (Biotecx) and stored at −70°C before use. Stage V–VI oocytes were obtained by partial ovariectomy of female *Xenopus laevis* oocytes (Xenopus-I or NASCO), anesthetized with tricaine methanesulfonate (1.5 g/liter, adjusted to pH 7.0 with NaOH). Oocytes were defolliculated by incubation in OR2 solution (82.5 mM NaCl, 2 mM KCl, 1 mM $MgCl_2$, and 5 mM HEPES, adjusted to pH 7.5 with NaOH) containing 2 mg/ml collagenase type II and 2 mg/ml hyaluronidase type II (Sigma Chemical Co.) for 90 min and another 90 min in a fresh enzyme solution at room temperature. Oocytes were injected with 0.5–1 ng of cRNA and incubated at 19°C in 2× diluted Leibovitz medium (Life Technologies, Inc.) for 1–4 d before measurements were made. For patch-clamp experiments, oocytes were subjected to a hypertonic shrinking solution containing 200 mM sucrose, thereby allowing the vitelline membrane to be easily removed.

Two-Electrode Voltage Clamp

Whole-oocyte current–voltage relationships were obtained in intact oocytes, using a two-electrode voltage clamp with 1 M KCl-filled current and voltage electrodes. Currents were recorded for 50 ms at each voltage, using a pulse protocol in which membrane potential was stepped by 10 mV, interspersed with a return to the resting membrane potential. The 5-K bath solution contained (mM): 105 NaCl, 5 KCl, 2 $CaCl_2$, 1 $MgCl_2$, and 5 HEPES, pH 7.4. The 5-Rb bath solution contained 5 mM RbCl instead of KCl.

Patch Clamp

Oocytes were bathed in a solution containing (mM): 110 KCl, 2 $CaCl_2$, 1 $MgCl_2$, and 5 HEPES, pH 7.4. Patch-clamp pipettes were pulled from borosilicate glass (7052; Richland Glass Co.) using a three-stage process and were coated with Sylgard. They were filled with solutions containing (mM): 110 KCl and 5 HEPES with or without 5 EDTA, pH 7.4. In some cases, KCl was substituted with NH_4Cl, RbCl, or $TlNO_3$. When Tl^+ was the major conducted ion, NO_3^- was substituted for Cl^- in the bath solution. All experiments were performed at room temperature (19–21°C). Pipette resistances were 1–3 MΩ. Currents were recorded with a patch-clamp amplifier (EPC-7; List Electronik) and stored, unfiltered, on videotape. For off-line analysis, current records were replayed from videotape, filtered at 1 kHz, and sampled at 5 kHz, using an Atari-based data acquisition system (Instrutech Corp.). Construction of open- and closed-time histograms and fitting with exponential distributions were carried using the TAC program (Sigworth and Sine, 1987).

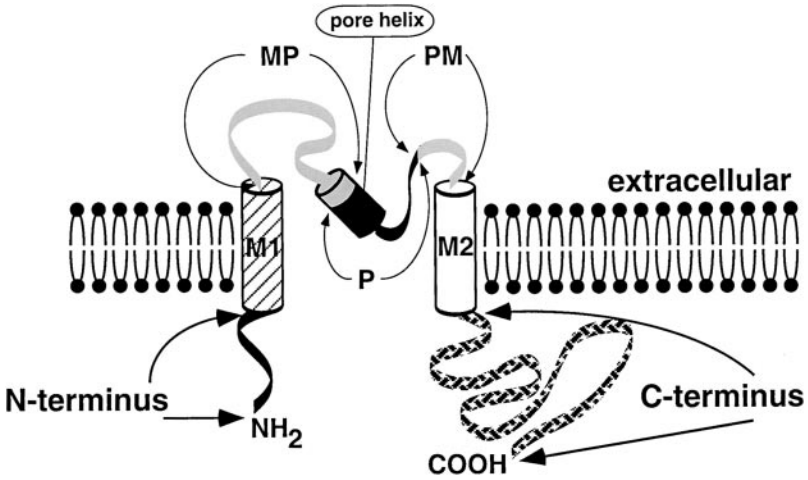

Figure 1. Segmental division of both ROMK and IRK. In each of the four subunits, M1 and M2 are presumed membrane-spanning domains. P denotes the highly conserved (pore) domain. The segments MP and PM are, respectively, the region between M1 and P, and the region between P and M2. The cylinder in the extracellular loop is the pore helix (Doyle et al., 1998), consisting of the first half of the P region with a minor contribution from the MP region. The seven segments of the chimeras are defined in Figure 4 of Choe et al. (1999).

Two-Ion Three-Site Four-Barrier Kinetic Model

We constructed a two-ion three-site four-barrier permeation model using matrix methods for steady state I-V curve computation (Begenisich and Cahalan, 1980). The transition rates were constructed based on the transition state theory. The transition rate from state i to j, k_j^i is given by Eq. 1:

$$k_j^i = \upsilon \cdot \exp\left(-\frac{\Delta E_A + z \cdot e \cdot \delta \cdot V}{k_B T}\right), \tag{1}$$

where ν and ΔE_A represent the Kramers' preexponential factor and the voltage-independent component of the transition state energy (between the binding site and the barrier peak), respectively. Other symbols have their usual meanings. No Coulombic interaction between ions was considered.

There are 27 ion-occupied states in this model. Since we are interested in the steady state, the transition-rate equations of the 27 states are given by Eq. 2:

$$\begin{bmatrix} -\sum_{j=2}^{27} k_j^1 & k_1^2 & \dots & k_1^{27} \\ k_2^1 & -\sum_{j=1, j\neq 2}^{27} k_j^2 & \dots & k_2^{27} \\ \vdots & \vdots & \vdots & \vdots \\ k_{27}^1 & k_{27}^2 & \dots & -\sum_{j=1}^{26} k_j^{27} \end{bmatrix} \cdot \begin{bmatrix} W_1 \\ W_2 \\ \vdots \\ W_{27} \end{bmatrix} = 0 \tag{2}$$

with the conservation equation:

$$\sum_{i=1}^{27} W_i = 1, \tag{3}$$

where W_i represents occupancy, a probability of finding the system in state i.

Since the leftmost matrix is singular, for computational purposes, a nonhomogeneous equation and a nonsingular matrix are produced by dropping the equation from the last row of the matrix and substituting Eq. 3. Then (Eq. 4):

$$\begin{bmatrix} W_1 \\ \vdots \\ W_{27} \end{bmatrix} = \begin{bmatrix} -\sum_{j=2}^{27} k_j^1 & k_1^2 & \dots & k_1^{26} & k_1^{27} \\ \vdots & \vdots & \vdots & \vdots & \vdots \\ k_{26}^1 & k_{26}^2 & \dots & -\sum_{j=1, j\neq 26}^{27} k_j^{26} & k_{26}^{27} \\ 1 & 1 & \dots & 1 & 1 \end{bmatrix}^{-1} \cdot \begin{bmatrix} 0 \\ \vdots \\ 0 \\ 1 \end{bmatrix}. \tag{4}$$

The inverse matrix was obtained using the "MINVERSE" function, a built-in function of Microsoft Excel (Microsoft Corp.). A specific occupancy of state i can be obtained using the "INDEX" function; for example, W_i = INDEX [MINVERSE (array), i, 27].

The current of a particular ion is its steady state net flux crossing over any one barrier multiplied by its valence. Therefore (Eq. 5):

$$\begin{aligned} \text{Net Current} &= \text{Current (ion A)} + \text{Current (ion B)} \\ &= e \cdot F \cdot \{z_A \cdot [(W_{EAE} + W_{EAA} + W_{EAB}) \cdot k_{AEE}^{EAE} \\ &\quad - (W_{AEE} + W_{AEA} + W_{AEB}) \cdot k_{EAE}^{AEE}] \\ &\quad + z_B \cdot [(W_{EBE} + W_{EBB} + W_{EBA}) \cdot k_{BEE}^{EBE} \\ &\quad - (W_{BEE} + W_{BEB} + W_{BEA}) \cdot k_{EBE}^{BEE}]\}, \end{aligned} \tag{5}$$

where z_A and z_B represent charge of ion A and ion B, respectively. The symbol EAE indicates the state that the second energy well is occupied by ion A, and the symbol EAA indicates the state that the second and the third energy wells from outside are occupied by ion A, and so on. Other symbols have their usual meanings.

All the fitting procedures were done using the "Solver" function, a built-in optimization function of Microsoft Excel. Results of the fitting process were displayed as both energy profile diagrams and transfer rates between energy wells. The energy profiles diagrams with peaks and wells have the advantage of providing a pictorial representation of the permeation process. Transfer rates have the advantage of being independent of model assumptions about absolute barrier height, or, equivalently, of the "preexponential factor."

RESULTS

Conductances of ROMK, IRK, and Chimeras

Channels were expressed by injecting cRNA into *Xenopus* oocytes, and patch-clamp recordings of single channels were obtained in the cell-attached mode. We were interested in whether the COOH terminus and the pore region contribute independently to the channel conductance. To address this question, we systematically measured the K^+ conductance of various chimeras. Fig. 2 shows current traces of ROMK2, IRK1, and some of the chimeras at −100 mV. ROMK2 has a larger open-channel current (−3.7 pA) than IRK1 (−2.8 pA) under these conditions. The K^+ conductance of IRK1 in this study is 29 pS, which is consistent with a previous study (Sabirov et al., 1997), but slightly larger than some other measurements; e.g., 23 pS (Kubo et al., 1993). These differences can be explained by different concentration of Mg^{2+} in the pipette solution: in our study, no Mg^{2+} was added, whereas Kubo et al. (1993) used 3 mM Mg^{2+}. 5 mM Mg^{2+} decreased single-channel conductance of IRK1 to 13 pS (Sabirov et al., 1997).

When the NH_2 terminus of ROMK was replaced with the corresponding region of IRK1, the current amplitude of the chimera (Chm1) was not changed significantly. However, when the ECL (consisting of MP, P, and PM regions) of ROMK was replaced, the chimera (Chm107) had larger currents (−6.3 vs. −3.7 pA at −100 mV). Replacement of the COOH terminus of ROMK2 with that of IRK1 (Chm13) decreased the current amplitude to −2.2 pA. These results are consistent with those of a previous study involving ROMK1–IRK1 chimeras (Taglialatela et al., 1994).

When the M1 or M2 region of IRK1 was replaced with that of ROMK2 (Chm4 and Chm12, respectively), there was no significant change (Fig. 2). However, when the ECL of IRK1 was converted to that of ROMK2 (Chm108), the current decreased from −2.8 to −2.0 pA.

In a summary of inward conductances (Fig. 3), the COOH terminus and the ECL stand out as major determinants of this conductance. As indicated in Fig. 3, the wild-type and chimeric channels can be classified into

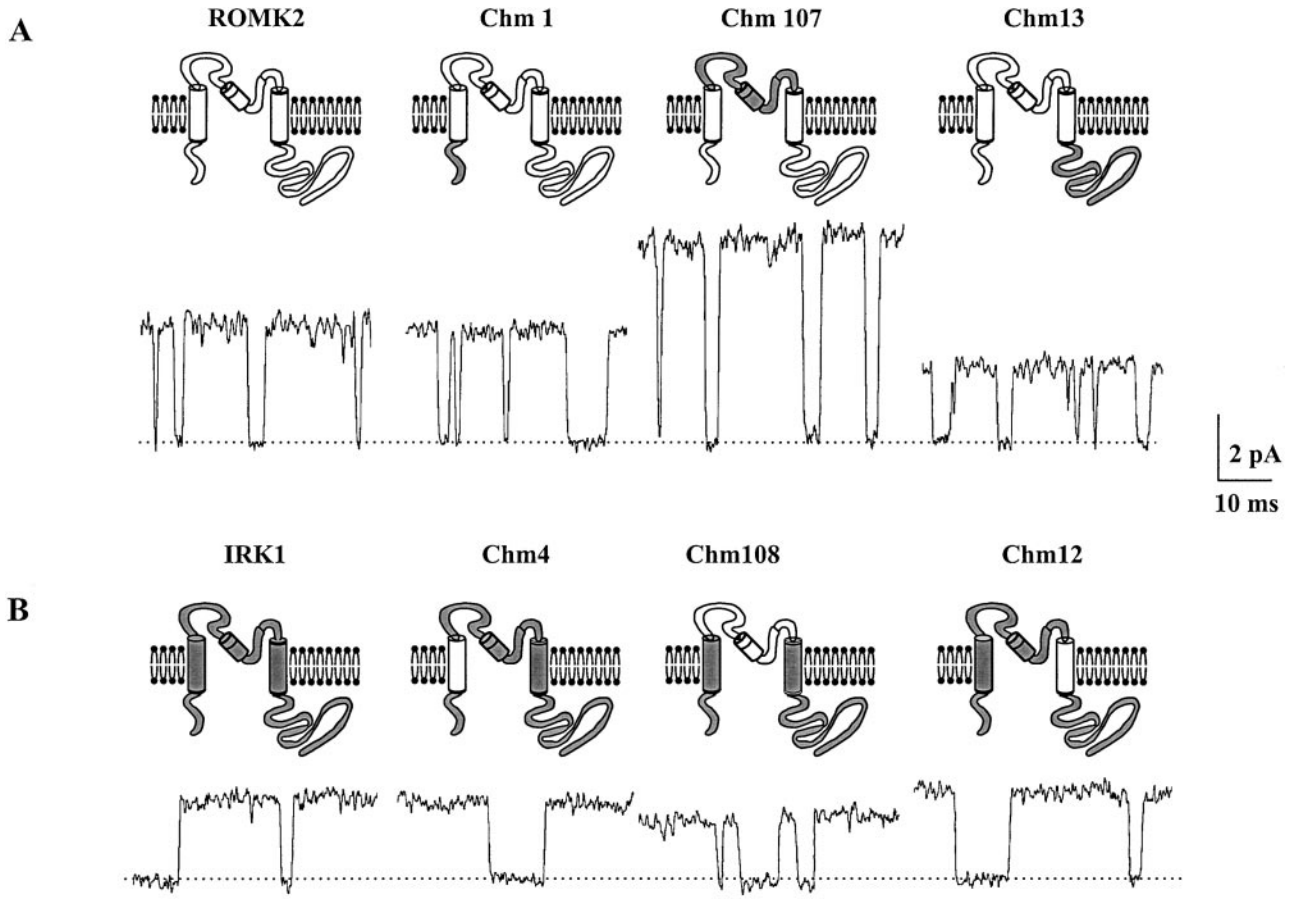

Figure 2. Single-channel current traces of ROMK2, IRK1, and some chimeras at −100 mV in the cell-attached mode. The shaded regions of the rectangles depicting the chimeras are derived from IRK1 and the open regions from ROMK2. The dotted lines indicate the closed state, and upward direction is inward current. The pipette solution contained 110 mM KCl. (A) Conductances of Chm107 and Chm13 are, respectively, larger and smaller than that of ROMK2. (B) Conductance of Chm108 is smaller than that of IRK1.

four groups, depending on the origin of these two components. Group 1 has both the ECL and the COOH terminus from ROMK2. Group 2 has both regions from IRK1. Group 3 has the ECL from ROMK2 and the COOH terminus from IRK1. Finally, Group 4, which shows the largest conductance (63 pS) has the ECL from IRK1 and the COOH terminus from ROMK2. M2 may also contribute somewhat because, in Group 2, the chimeras that have M2 from ROMK2 have slightly higher conductances than those with the M2 from IRK1. However, in the subsequent analysis, we will focus only on the ECL and the COOH terminus because these regions have the largest effects.

The simplest model that can explain these results is one in which the conduction pathway has two regions that impede ion flow (resistors) arranged in series (see discussion and Fig. 8). The "outer" resistor is formed by the extracellular region, and the "inner" resistor by the COOH terminus. In this model, the inner resistance of IRK1 was larger than that of ROMK2, while the outer resistance of ROMK2 was larger than that of IRK1.

3P[2] Is Responsible for the Conductance Difference in the Extracellular Region

Chimeras were constructed to evaluate which region of the ECL is the primary determinant of conductance. In our scheme (Choe et al., 1999), the ECL is divided into three parts: (a) the most conserved, pore forming, P region, (b) the MP region, between M1 and P, and (c) the PM segment, between P and M2 (Fig. 1). These chimeras showed that exchanging the P region of ROMK2 with that of IRK1 increased the conductance to an even greater extent than exchanging the entire ECL (Fig. 4). The difference is attributable to MP, since chimeras where this segment was derived from IRK1 had lower conductances.

The P regions of ROMK2 and IRK1 have only two amino acid differences. One is at the −1P position and

[2]To compare positions in the P-regions between different K channels, we follow the numbering scheme used in the *Shaker* channel (Heginbotham et al., 1994); TXXTXGYG, the signature sequence of the K channels, are designated as 1P through 8P.

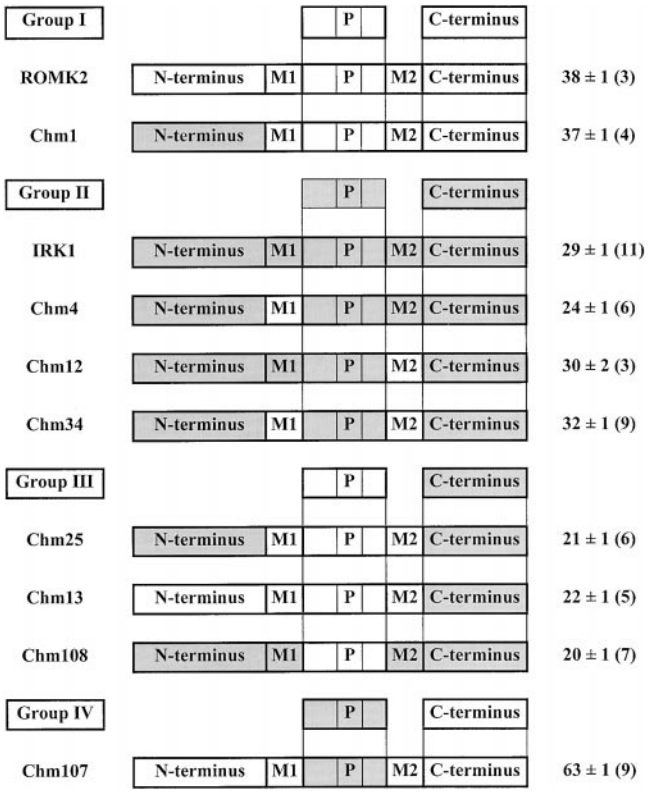

Figure 3. Conductance (pS) at the voltage range of 0–100 mV. Shaded rectangles correspond to segments from IRK1. Clear rectangles denote segments from ROMK2. Data are means ± SEM (number of measurements).

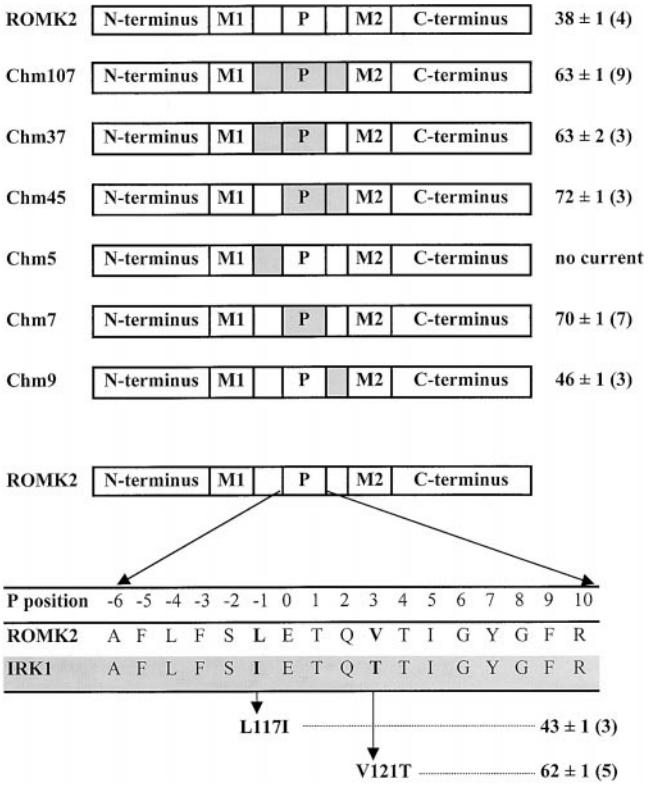

Figure 4. K^+ conductance (pS) of ECL chimeras and mutants in the P region. Data are means ± SEM (number of measurements).

the other is at the 3P position. Therefore, we studied mutants in which either the −1P or 3P position in ROMK2 was changed to the corresponding amino acid of IRK1. The L117I mutant, involving the −1P position, had the same conductance as wild type, whereas the V121T mutant, involving the 3P position, had a conductance similar to that of Chm107 (Fig. 4), although slightly smaller than that of Chm7. Therefore, the 3P position seems to be responsible for most of the differences in conductances arising from different ECLs.

The NH_4^+, Rb^+, and Tl^+ versus K^+ Selectivities of ROMK2 and IRK1 Are Different

We also studied NH_4^+, Rb^+, and Tl^+ selectivities of single channels in the cell-attached mode. Fig. 5 shows current traces of ROMK2 and IRK1 for K^+, NH_4^+, Rb^+ and Tl^+. Replacing pipette K^+ with different ions alters the reversal potential in the hyperpolarizing direction for NH_4^+ and Rb^+, and in the depolarizing direction for Tl^+. Bi-ionic potentials from linear-regression analysis of the data and permeability ratios are shown in Table I. The overall permeability sequence for both ROMK2 and IRK1 is $Tl^+ > K^+ > Rb^+ > NH_4^+$. Permeability ratios of NH_4^+, Rb^+, Tl^+, versus K^+ for both ROMK2 and IRK1 are similar.

To quantitatively estimate the inward slope conductance, we measured current amplitudes at voltages of up to 100 mV negative to the reversal potentials: 0 to −100 mV for K^+, −60 to −160 mV for NH_4^+, −20 to −120 mV for Rb^+, and 20 to −80 mV for Tl^+ (Fig. 6). However, it was difficult to measure unitary events of Rb^+ current for IRK1 at voltages positive to −120 mV, so we increased the voltage range to −200 mV to obtain a single-channel current of −0.6 pA. Tl^+ ion currents in IRK1 often opened to a maximal level, and then declined, sometimes gradually, to the main conductance level (Fig. 5). Because we don't know the mechanism underlying this phenomenon, for the analysis of Tl^+ conductance, we took the main conductance state, although the conclusions reached are the same if the maximum current levels are used. Although inward slope conductances were determined from a linear-regression analysis, the I-V plots in Figs. 6 and 7 deviate slightly but consistently from linearity. The data can be explained by kinetic models with at least three energy barriers and two energy wells (see Fig. 9, and see also Choe, 1999). The main points of this paper, however, can be adequately illustrated with simple linear resistive elements.

The conductance ratios of NH_4^+, Rb^+, or Tl^+ versus K^+ for ROMK2 and IRK1 are shown in Table I. The conductance sequence for ROMK2 is: $NH_4^+ > K^+ > Tl^+ > Rb^+$. For IRK1, the conductance sequence is: $K^+ >$

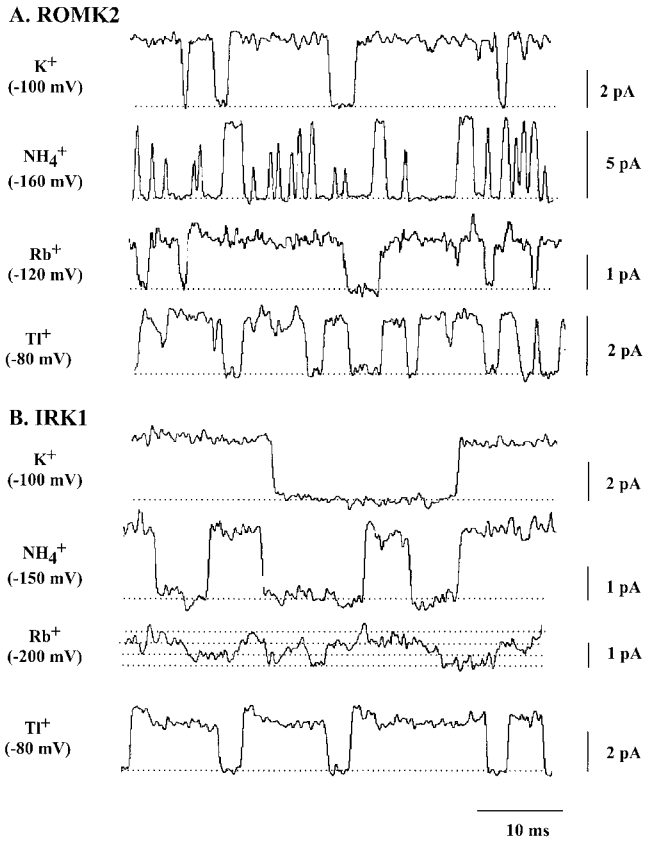

Figure 5. Single-channel current traces of ROMK2 and IRK1 with K^+, NH_4^+, Rb^+, and Tl^+ in the pipettes (110 mM) in the cell-attached mode. The dotted lines indicate the closed state, and upward deflections denote inward current. The voltages in parentheses indicate the membrane potentials. The Rb^+ currents for IRK1 were recorded from patches with multiple channels.

TABLE I

Selectivities of ROMK2, IRK1, and Mutants

	X	γ	γ_x/γ_K	E_{rev}	P_x/P_K	*n*
ROMK2	K^+	38 ± 1	1	−2 ± 1	1	4
	NH_4^+	62 ± 2	1.62	−63 ± 1	0.09	3
	Rb^+	15 ± 1	0.38	−25 ± 2	0.42	4
	$T1^+$	21 ± 1	0.53	19 ± 2	2.30	3
IRK1	K^+	29 ± 1	1	−3 ± 1	1	10
	NH_4^+	17 ± 2	0.59	−63 ± 1	0.10	9
	Rb^+	3 ± 1	0.10	−21 ± 1	0.49	4
	$T1^+$	24 ± 1	0.83	15 ± 1	1.84	4
Chm107	K^+	63 ± 1	1	−4 ± 1	1	9
	NH_4^+	57 ± 4	0.91	−61 ± 1	0.11	3
	Rb^+	9 ± 1	0.14	−22 ± 3	0.50	3
	$T1^+$	23	0.37	17	2.30	2
Chm25	K^+	21 ± 1	1	−6 ± 2	1	4
	NH_4^+	46 ± 2	2.13	−66 ± 2	0.09	6
	Rb^+	10 ± 1	0.47	−6 ± 1	0.49	5
	$T1^+$	18 ± 2	0.82	15 ± 1	2.23	4
Chm1	K^+	37 ± 1	1	0 ± 1	1	4
	$T1^+$	19 ± 1	0.51	18	2.04	6
Chm13	K^+	22 ± 1	1	0 ± 2	1	5
	$T1^+$	15 ± 1	0.65	16 ± 1	1.91	7
Chm8	K^+	16 ± 1	1	−4 ± 1	1	4
	NH_4^+	53 ± 1	3.38	−62 ± 1	0.10	4
	Rb^+	10 ± 1	0.61	−22 ± 1	0.43	3
L117I	K^+	43 ± 1	1	−3 ± 1	1	3
	NH_4^+	66 ± 1	1.55	−63 ± 1	0.10	3
	Rb^+	15	0.36	−25	0.42	1
V121T	K^+	66 ± 1	1	−4 ± 1	1	3
	NH_4^+	39 ± 1	0.59	−62 ± 1	0.09	3
	Rb^+	6 ± 1	0.09	−20 ± 4	0.52	3

Data are means ± SEM. *n*, number of measurements.

$Tl^+ > NH_4^+ >> Rb^+$. Thus, the conductance ratios of ROMK and IRK differ in sequence order. Also, the conductance and permeability ratios of channels are different. The most striking examples are for the NH_4^+ and Tl^+ selectivity of ROMK2: $\gamma_{NH4}{}^+/\gamma_K{}^+$ is 1.62, whereas $P_{NH4}{}^+/P_K{}^+$ is 0.09; $\gamma_{Tl}{}^+/\gamma_K{}^+$ is 0.53, whereas $P_{Tl}{}^+/P_K{}^+$ is 2.30.

The ECL Controls Differences in NH_4^+ and Rb^+ Selectivity, while the Two Cytoplasmic Termini Control Tl^+ Selectivity

To identify the regions responsible for the selectivity differences between ROMK2 and IRK1, we studied the selectivities of two representative chimeras, Chm25 (having the NH_2 and COOH termini of IRK1) and Chm107 (having the ECL of IRK1). Fig. 6 shows I-V plots of these chimeras, as well as those of wild-type ROMK2 and IRK1. Table I summarizes the selectivities of these chimeras. The permeability sequence of both Chm25 and Chm107 is: $Tl^+ > K^+ > Rb^+ > NH_4^+$, which is similar to that of ROMK2 and IRK1. However, the conductance ratio sequences for Chm25 and Chm107 are: $NH_4^+ > K^+ > Tl^+ > Rb^+$ and $NH_4^+ \approx K^+ > Tl^+ > Rb^+$, respectively. The latter differs from those of both ROMK2 and IRK1.

In both cases, the ratios $\gamma_{NH4}{}^+/\gamma_K{}^+$ and $\gamma_{Rb}{}^+/\gamma_K{}^+$ of the chimeras are closer to those of the wild-type channel from which the ECL of the chimera was derived. However, the Tl^+ versus K^+ conductance ratio appeared to be determined by a different region. The $\gamma_{Tl}{}^+/\gamma_K{}^+$ of Chm25 and Chm107 more closely resemble those of the wild-type channel from which the cytoplasmic termini were derived. Thus $\gamma_{Tl}{}^+/\gamma_K{}^+$ for Chm107 is 0.37, closer to the value for ROMK2 (0.52). Conversely, $\gamma_{Tl}{}^+/\gamma_K{}^+$ for Chm25 is 0.82, closer to the value for IRK1 (0.83).

To identify the terminus responsible for Tl^+ ion selectivity, we tested the Tl^+ ion conductance of Chm1 and Chm13. These chimeras are, respectively: ROMK2 with the NH_2 terminus of IRK1 and ROMK2 with the COOH terminus of IRK1 (Table I). The Tl^+ and K^+ conductances of Chm1 are similar to those of ROMK2. However, the conductances of Chm13 are closer to those of Chm25. These results, together with the effect of COOH

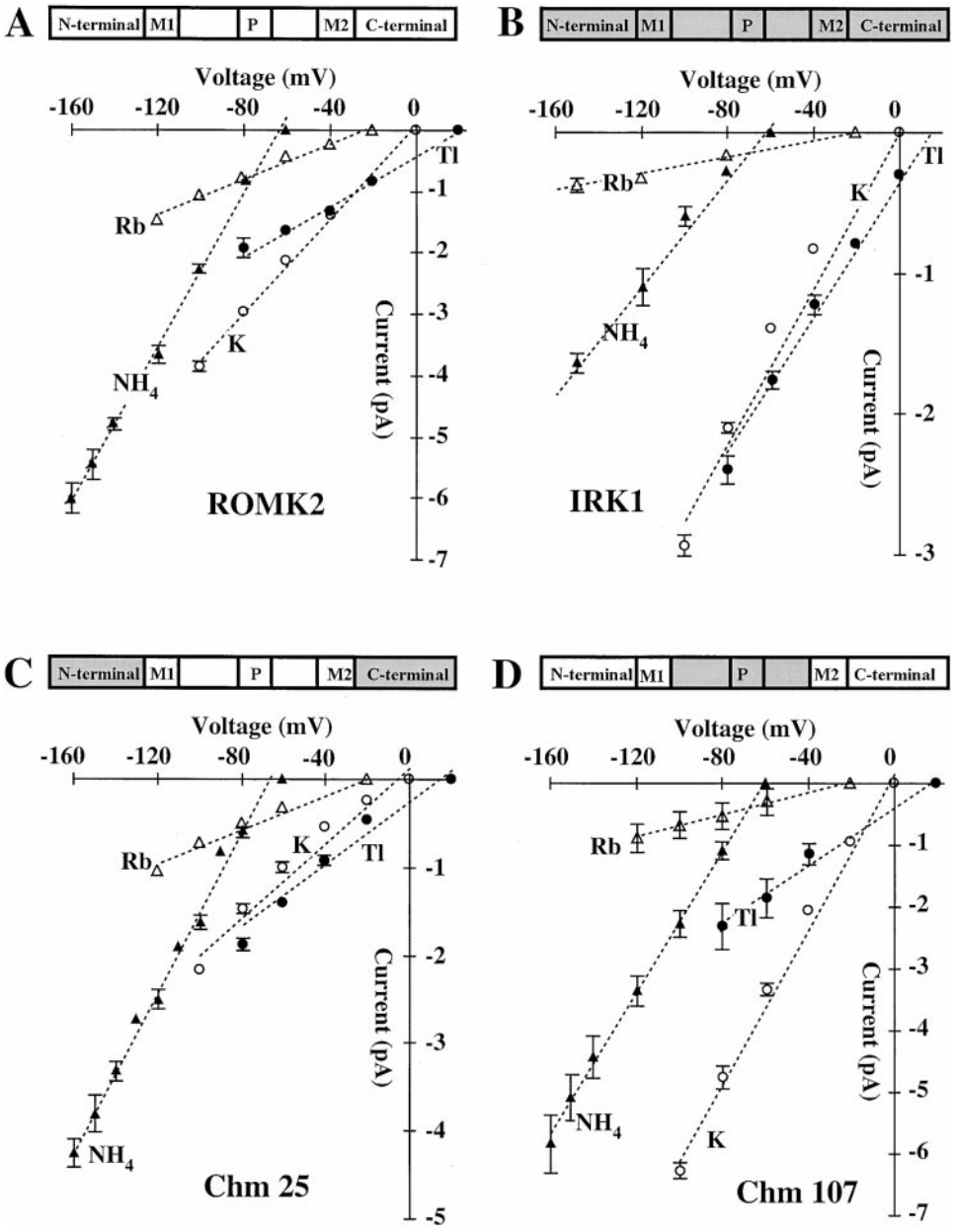

Figure 6. I-V plots for single channel inward currents of ROMK2, IRK1, Chm25, and Chm107 in the cell-attached mode. Data points and error bars for the four cations in the pipette represent means ± SEM as follows: K^+ (○), NH_4^+ (▲), Rb^+ (△), and Tl^+ (●). The dashed lines are averages of linear regressions of individual patches over the following ranges: 0 to −100 mV (K^+), −60 to −160 mV (NH_4^+), −20 to −120 mV (Rb^+ for ROMK2), −20 to −200 mV (Rb^+ for IRK1), and 20 to −80 mV (Tl^+). The correlation coefficients are (in the order of K, NH_4, Rb, and Tl): for ROMK2: 0.997, 0.998, 0.989, and 0.991; for IRK1: 0.989, 0.988, 0.996, and 0.993; for Chm25: 0.987, 0.999, 0.987, and 0.984; for Chm107: 0.996, 0.999, 0.993, and 0.993.

terminus on K^+ conductance, suggest that the Tl^+ versus K^+ selectivity is controlled mainly by the COOH terminus.

3P Is Also Responsible for NH_4^+ and Rb^+ Selectivity Differences

To identify the segments of the ECL responsible for K^+:Rb^+ selectivity, we tested the macroscopic Rb^+ versus K^+ conductance ratio of chimeras using the two-electrode voltage clamp technique. When the bath solution was switched from 5 K^+ to 5 Rb^+ solution, the chimeras having the P region of ROMK2 (Chm8 and 9) had $G_{Rb^+}/G_{K^+} = 0.45 \sim 0.51$, similar to that (0.44) of ROMK2 wild type; whereas the chimeras having the P region of IRK1 (Chm6, 7, 10, 37, and 45) had $G_{Rb^+}/G_{K^+} = 0.05 \sim 0.17$, similar to that (0.05) of IRK1 wild type. These results suggest that the P region is important for the Rb^+ versus K^+ selectivity.

Therefore, we evaluated only Chm8 and the two point mutants, L117I and V121T, to narrow down the determinant of the single-channel conductance ratio of Rb^+ and NH4 versus K^+. These results are shown in Fig. 7 and Table I. Both Chm8 (which is IRK1 except for the P region of ROMK2) and the point mutant L117I have a single-channel conductance sequence of $NH_4^+ > K^+ > Rb^+$, similar to that of ROMK2. The conductance sequence of the V121T mutant was $K^+ > NH_4^+ >> Rb^+$, a sequence identical to that of IRK1. Therefore, we conclude that the 3P position of IRK and ROMK is responsible for the selectivity differences among the cations: K^+, Rb^+, and NH_4^+.

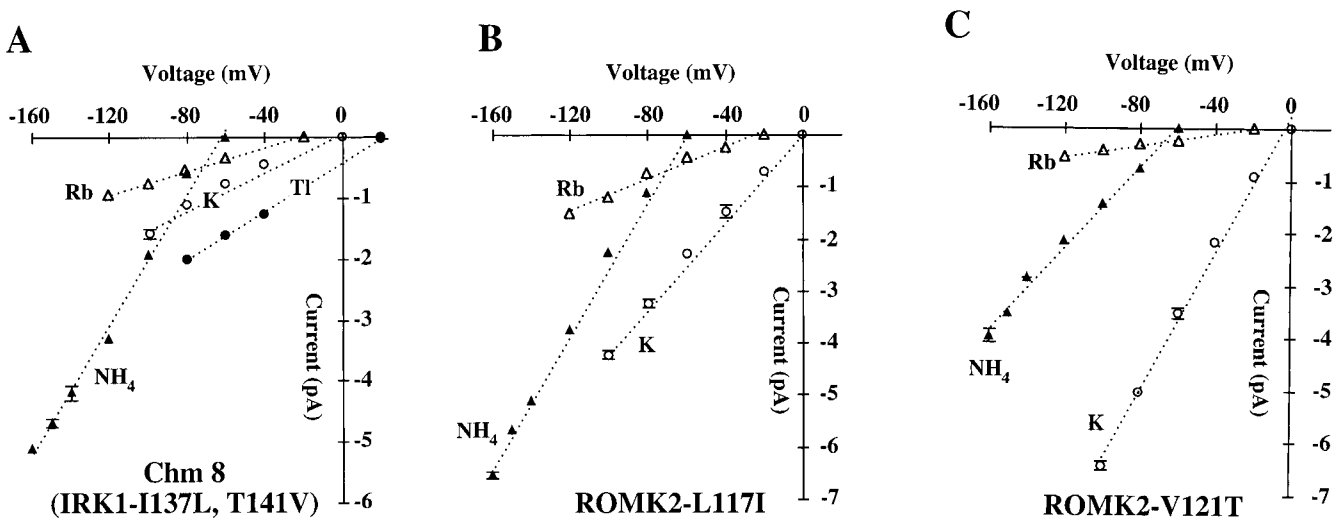

Figure 7. I-V plots for single channel inward currents of Chm8 (ROMK2, L117I, and V121T) and the individual mutants, L117I and V121T, in the cell-attached mode. The symbols and the voltage range for the conductance estimates are the same as in Fig. 6. The correlation coefficients are (in the order of K, NH_4, and Rb): for Chm8: 0.994, 0.993, and 0.991; for L117I: 0.997, 0.998, and 0.991; for V121T: 0.997, 0.996, and 0.994.

3P Position Mutations

Since the 3P position is very important for determining the conductances of K^+, NH_4^+, and Rb^+ of the channels, we substituted the Val residue at this position in ROMK2 with 18 other amino acids to further understand the molecular mechanism of conductance and selectivity.

We observed no significant current from 10 mutants in which the V121 residue (3P position) was replaced with one of the following: Asp, Glu, Lys, Arg, Tyr, Pro, Trp, Phe, Gly, or Leu. The Leu mutant had a resting membrane potential of −70 mV at 5 mM K^+ bath solution, consistent with K^+ channel expression, but had <1 μA of current at a voltage of −120 mV. This is puzzling since Ile, a similar amino acid, formed a fully functional channel. In the other nine mutants, the potential was −30 to −50 mV even 3 d after cRNA injection, which is similar to that of noninjected oocytes. Since none of the charged amino acids showed significant currents except for histidine, we expect that the histidine exists in the deprotonated form at least when the channel is conducting. In the cases of Tyr, Trp, and Phe, the large size of the side chains might occlude the pore. The absence of current of the Pro mutant may result from a structural modification since this side chain changes the direction of peptide backbone abruptly.

The remaining nine mutants, together with ROMK2, expressed currents that were large enough for single-channel analysis. The conductances and selectivities of these channels are presented in Table II. The first five rows summarize results with the five nonpolar side chains (Val, His, Met, Ile, and Ala). These, together with two of the polar side chain mutants (Gln and Cys) shown in the next two rows, had an ROMK2-type conductance sequence: $NH_4^+ > K^+ > Rb^+$. On the other hand, two of the mutants with polar side chains (Thr and Ser) at position 121 had an IRK1-type conductance sequence: $K^+ > NH_4^+ > Rb^+$. Finally, the mutant with Asn at this position showed a novel selectivity sequence: $NH_4^+ > Rb^+ > K^+$.

DISCUSSION

The ECL and COOH Terminus Behave as Two Resistors in Series

While the inward single-channel K^+ conductances of ROMK2 and IRK1 are similar, this can be viewed as the net result of opposite contributions of two parts of the channels. The ECL of IRK1, including the P region, has a much higher conductance than that of ROMK2, whereas having the COOH terminus of IRK1 lowers the conductance. Exchanging the ECLs and COOH termini of the two channels changes the overall conductance in a way that suggests that these two parts of the channels form independent resistances. The simplest interpretation of these results is that the COOH terminus, perhaps in combination with other elements of the channel, forms the inner part of the conductive pore, which can confer a resistor in series with that of the P region (Fig. 8). Another interpretation of the result is that replacement of COOH terminus affects the structure of selectivity filter through propagation of a conformational change. However, this idea does not predict the observation that replacing the COOH terminus of ROMK with that of IRK increases channel resistance by an amount equal to the decrease observed when the converse exchange is made. It is also difficult

TABLE II

Single-Channel Conductances of Various Mutations at the V121 Position of ROMK2

		K^+	NH_4^+	Rb^+
ROMK2	γ_X	38 ± 1 (4)	62 ± 2 (3)	15 ± 1 (4)
	γ_X/γ_{K^+}	1	1.6	0.4
V121H	γ_X	27 ± 2 (3)	56 ± 1 (3)	12 ± 1 (3)
	γ_X/γ_{K^+}	1	2.1	0.5
V121M	γ_X	8 ± 1 (3)	19 ± 2 (3)	4 ± 1 (3)
	γ_X/γ_{K^+}	1	2.2	0.5
V121I	γ_X	25 ± 1 (3)	52 ± 3 (3)	9 ± 1 (3)
	γ_X/γ_{K^+}	1	2.1	0.4
V121A	γ_X	15 ± 1 (3)	52 ± 2 (3)	13 ± 1 (3)
	γ_X/γ_{K^+}	1	3.4	0.8
V121Q	γ_X	13 ± 1 (4)	37 ± 2 (4)	6 ± 1 (1)
	γ_X/γ_{K^+}	1	2.8	0.5
V121C	γ_X	6 ± 1 (4)	22 ± 1 (3)	5 ± 1 (3)
	γ_X/γ_{K^+}	1	3.6	0.8
V121T	γ_X	66 ± 1 (5)	39 ± 1 (3)	6 ± 1 (3)
	γ_X/γ_{K^+}	1	0.6	0.1
V121S	γ_X	63 ± 1 (3)	58 ± 3 (3)	10 ± 1 (3)
	γ_X/γ_{K^+}	1	0.9	0.2
V121N	γ_X	12 ± 1 (3)	71 ± 2 (3)	20 ± 1 (3)
	γ_X/γ_{K^+}	1	5.9	1.7

Data are means ± SEM. Number of measurements are in parenthesis.

to reconcile with the fact that changing the COOH terminus alters the conductance of the channel without affecting the striking selectivity patterns among the permeant cations K^+, NH_4^+, and Rb^+ (Table I and Fig. 6).

One prediction made from the series resistors model is that in ROMK2, with a relatively large outer resistor and a relatively small inner resistor, the voltage drop across the outer resistor should be smaller than that across the same region of IRK1. In principle, this voltage drop can be estimated using a blocking ion that binds to a site between the two resistors. Mg^{2+} is one candidate for such a blocker. It reduces the single-channel conductance of IRK1 and ROMK2 when added to the cytoplasmic side of the membrane (Lu and MacKinnon, 1994; Wible et al., 1994; Chepilko et al., 1995), and its affinity depends on electrostatic interactions with amino acid side chains in the M2 segment (Fakler et al., 1994; Lu and MacKinnon, 1994; Wible et al., 1994), which should lie between the two resistors. Mg^{2+} block has a voltage dependence consistent with a binding site within the electric field. In the cases of ROMK and other weak inward-rectifier K^+ channels, the apparent fraction of the field sensed at that site (δ_{Mg}) is 0.28–0.44 of the total measured from the cytoplasmic side (Horie et al., 1987; Lu and MacKinnon, 1994; Nichols et al., 1994; Chepilko et al., 1995; Spassova and Lu, 1998). For IRK1 and other strong inward-rectifier K^+ channels, δ is higher, ranging from 0.56 to 1.01 from the cytoplasmic side (Matsuda, 1988; Horie and Irisawa, 1989; Lopatin et al., 1994; Stanfield et al., 1994; Wible et al., 1994; Yang et al., 1995a), except for one study that reported a value of 0.33 (Fakler et al., 1994). These numbers are in general agreement with the model. If $\delta_{Mg} = 0.3$ for ROMK2, the ratio of inner to outer resistors (R_i/R_o) would be $0.3/0.7 = 0.43$. Since the resistance of a single channel is $(38\ pS)^{-1}$ or 26 GΩ, R_i will equal 8 GΩ and R_o will equal 18 GΩ. For IRK1, the corresponding values can be calculated from the difference in resistance when the ECL or COOH terminus of ROMK2 is replaced with the corresponding part of IRK. This gives $R_i = 27$ GΩ and $R_o = 8$ GΩ. This predicts $\delta_{Mg} = 8/35 = 0.77$, within the range of measured values.

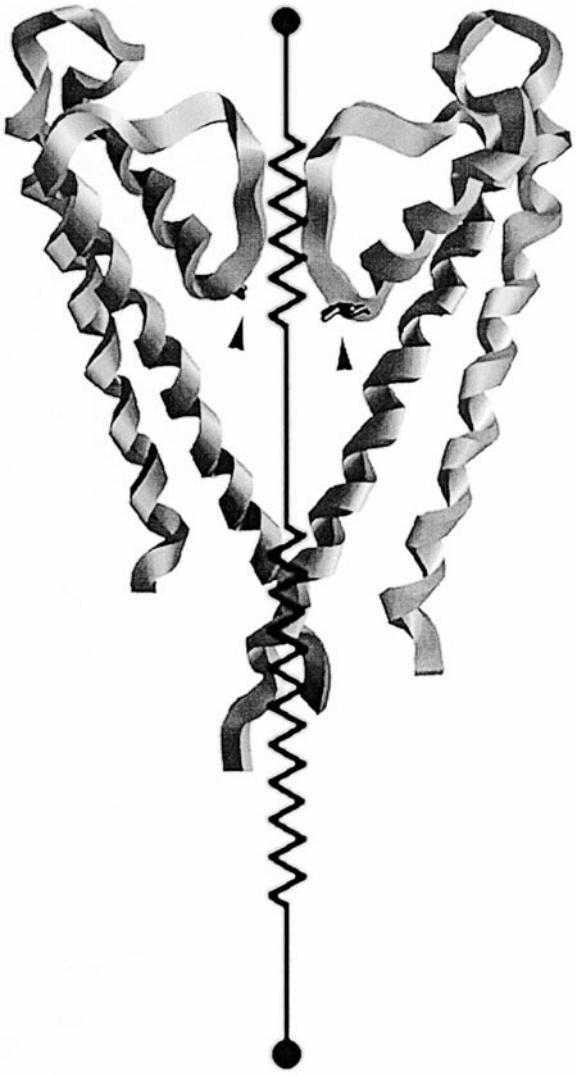

Figure 8. The 3P position in the crystal structure of the KcsA channel (arrows) is located at the COOH terminus of the pore helix. The 3P residue in KcsA and IRK is Thr; in ROMK it is Val. The KcsA ribbon model was constructed from coordinates downloaded from the PDB database, structure 1BL8. Two of the four subunits are shown for clarity. The symbol for two resistors is superimposed on the channel structure. Note that the model assumes a long cytoplasmic inner resistor that is not observed in the channel structure.

Mg^{2+} might not be the perfect blocker for this analysis. At least part of the voltage dependence of Mg^{2+} block has been attributed to the displacement of K^+ ions across the outer mouth of the channel (Spassova and Lu, 1998). Thus, the apparent electrical distance for block may overestimate the true fraction of the field sensed at the binding site. However, even if the inner resistor of ROMK2 is small, that of IRK would be $\geq$19 GΩ, a significant fraction of the total. The inner pore is unlikely to be as narrow as the selectivity filter because other studies have indicated that large cations can enter the channel from the inside, suggesting that the opening of the pore to the cytoplasm is relatively wide. Polyamines such as spermine and spermidine block Kir channels in a voltage-dependent fashion from the inside (Lopatin et al., 1994, 1995; Taglialatela et al., 1995; Yang et al., 1995a; Lopatin and Nichols, 1996; Pearson and Nichols, 1998), indicating that the narrowest region of the inner pore must be at least as wide as the diameter of these molecules, which are $\sim$4-Å wide and 7–18-Å long.

A pore resistance, R_{pore}, is determined by several factors (Eq. 6):

$$R_{pore} = \rho \frac{l}{\pi \cdot a^2}, \quad (6)$$

where ρ, l, and a represent resistivity, the length, and the radius of the pore, respectively. The high inner resistance presumably reflects several possibilities: a long extension of the pore into the cytoplasm, and/or a hydrophobic inner pore wall (which will increase resistivity). The possibility of hydrophobic wall of the inner pore is suggested by the finding that cations with longer hydrophobic elements can be more effective K^+ channel blockers (Armstrong, 1969; Armstrong, 1971). Indeed, the KcsA structure shows hydrophobic walls in the pore lined by the second transmembrane domain (Doyle et al., 1998). The wall of the inner pore, which was not determined in the KcsA structure, might be hydrophobic as well.

Another possibility is that the diameter of the inner pore fluctuates. By analogy, the x-ray structure of myoglobin reveals no path for O_2 to reach the heme group (Perutz and Mathews, 1966; Case and Karplus, 1979), but O_2 and CO bind to the heme group at rates that are close to the diffusion-controlled limit (Hasinoff, 1977), suggesting thermal fluctuations of the protein (Elber and Karplus, 1987). This mechanism would allow passage of a relatively large molecule through a normally narrow pore.

Kir Channels Have Different Relative Conductances of Permeant Cations

Table III lists the permeation and the conductance ratios of various native and cloned K^+ channels. All of these K^+ channels have remarkably similar permeability ratios (P_X/P_K), where $Tl^+ > K^+ > Rb^+ > NH_4^+$. Conductance ratios show a greater variation with channel type than do the permeability ratios. This is partly because conductance ratios depend on experimental conditions such as the voltage range over which they are measured. Nevertheless it is clear that different K^+ channels can have distinct selectivity sequences based on conductance ratios.

While the signature GYG sequence is thought to be the site conferring selectivity for K^+ ions over Na^+, the selectivity sequence for permeant ions may have different determinants because ROMK2 and IRK1 have the identical GYG sequence, but yet different selectivity based on the single-channel conductance ratio. Our results indicate that most of the conductance selectivity among the permeant cations (K^+, Rb^+, and NH_4^+) is conferred by the outer resistance. The one exception is that the Tl^+ versus K^+ single-channel conductance ratio follows the origin of the two cytoplasmic termini (Table I). If both termini originate from ROMK, the Tl^+/K^+ conductance ratio resembles that of ROMK2; if both termini originate from IRK, then the ratio resembles that of IRK1.

How can Tl^+/K^+ conductance ratio be altered by the relatively wide inner pore, whereas similar sized ions, Rb^+ and NH_4^+, are not affected? One possibility is that Tl^+ may bind to specific sites within the inner pore, such as sulfhydryl groups, and affect the Tl^+ conductance. A Tl^+ binding-site hypothesis was first proposed by Ashcroft and Stanfield (1983) to explain inactivation of Tl^+ current in frog skeletal muscle.

3P Position

We identified the 3P position (located 3 residues NH_2 terminal to the GYG signature sequence), as a modifying site for ion permeation through inward rectifiers. This is similar to what is observed with voltage-gated channels. For example, *Shaker* and mslo (Ca^{2+}-activated K^+) channels display significant differences in both $\gamma_{NH4}^+/\gamma_K^+$:0.75/0.18 and γ_{Rb}^+/γ_K^+:0.5/0.07 (Table III). These differences can be correlated with differences at the 3P position, where *Shaker* has a Thr residue and mslo has a Ser residue. In fact, the *Shaker* mutation T441S (at the 3P position) changed both the conductance and the bi-ionic permeability ratios for Rb^+ and NH_4^+ (Yool and Schwarz, 1991). This mutant also exhibited an anomalous mole fraction effect in P_{Rb}^+/P_K^+ (Yool and Schwarz, 1996). In our experiments, V121T and V121S showed no significant difference in selectivity. The 3P position is also responsible for the 10-fold difference in Ba^{2+} affinity between ROMK2 and IRK1 (Zhou et al., 1996). The homologous position in the *Shaker* K^+ channel was also shown to be important for the efficacy of block by extracellular Ba^{2+} (Harris et al., 1998).

The mechanism underlying the effect of changing the 3P amino acid on selectivity is unknown. Our analysis suggests that the outer resistor of the IRK1 channel conducts K^+ more easily than that of ROMK2, but that

TABLE III

Comparison of Selectivities between K^+ Channels

	PX/PK			GX/GK				
	NH_4^+	Rb^+	$T1^+$	NH_4^+	Rb^+	$T1^+$	Measurement	
Weak inward rectifier								
ROMK2	0.09	0.42	2.58	1.62	0.38	0.52	Single channel	This study
	0.12	0.63	1.56	1.00	0.36	0.70	Single channel	Chepilko et al., 1995
	0.13	0.71	—	—	0.48	—	Whole cell	Zhou et al., 1994
	0.27	0.76	—	0.46	0.23	—	Whole cell	Zhou et al., 1996
	—	0.82	—	—	—	—	Macropatch	Reuveny et al., 1996
KATP	—	0.76	—	—	—	—	Single channel	Spruce et al., 1987
Strong inward rectifier								
IRK1	0.10	0.49	1.49	0.59	0.10	0.94	Single channel	This study
	0.09	0.28	—	—	—	—	Whole cell	Sabirov et al., 1997
	—	0.68	—	—	0.09	—	Whole cell	Abrams et al., 1996
	—	0.68	—	—	—	—	Macropatch	Reuveny et al., 1996
CCD-IRK3	0.32	1.25	1.64	0.28	0.12	1.41	Whole cell	Welling, 1997
Starfish egg	0.04	0.35	1.50	—	<0.1	1.4	Whole cell	Hagiwara and Takahashi, 1974
Frog muscle	—	—	—	—	<0.1	—	Whole cell	Standen and Stanfield, 1980
	—	—	1.66	—	—	—	Whole cell	Ashcroft and Stanfield, 1983
Voltage-gated K^+ channel								
Shaker	0.09	0.66	—	0.75	0.50	—	Single channel	Heginbotham and MacKinnon, 1993
	0.11	0.89	—	—	—	—	Whole cell	Perez-Cornejo and Begenisich, 1994
Ca^{2+} activated	0.11	0.67	1.20	—	—	—	Single channel	Blatz and Magleby, 1984
	0.10	0.70	1.30	0.18	0.07	0.41	Single channel	Eisenman et al., 1986
Delayed rectifier	0.13	0.91	2.30	—	—	—	Whole cell	Hille, 1973
	0.15	0.74	1.29	—	—	—	Whole cell	Reuter and Stevens, 1980
L-type transient A	0.12	0.76		1.5	0.5	—	Whole cell	Shapiro and DeCoursey, 1991
	0.18	0.73	2.04	—	—	—	Whole cell	Taylor, 1987

both Rb and NH_4 conductances are smaller. This could be explained by a small decrease in the pore diameter of the selectivity filter, which would favor the conductance of the smaller K^+ ion over that of the larger Rb and NH_4 ions. It is also possible that electrostatic effects are involved. According to the x-ray crystal model of the related KcsA K^+ channel (Doyle et al., 1998), the 3P position is located at the COOH terminus of the pore helix, the end which points toward the pore (Fig. 8). Because an α helix has an associated macro dipole (Hol, 1985), changes at the 3P position may change the dipole and thereby affect the electric field within the pore. A stronger field might lower a critical energy barrier for K^+ more than that for the larger cations.

Three-Site Four-Barrier Model

The selectivity of ROMK2 for NH_4^+ versus K^+ is remarkably different for permeability and conductance ratios. NH_4 permeability was 10-fold smaller than that of K^+, but the conductance was 1.6-fold larger (Fig. 6 and Table I). To explain these contradictory results, we examined kinetic models of ion permeation. The purpose of this exercise was not to precisely determine energy profiles, but rather to check whether the simple model can account for the observed results. We used three-site four-barrier models because the x-ray diffraction of a bacterial K^+ channel crystal showed three discrete electron densities along the pore in single-file manner (Doyle et al., 1998). Also, the three-site four-barrier model gives a better fit for NH_4^+ I-V data than the two-site three-barrier model (although two-site three-barrier model gives the same general conclusion).

First, we obtained depths and heights of energy wells and peaks for the K^+ ion energy profile that predicted the I-V relationship for the K^+ ion permeation. For simplicity, we used equally spaced wells and barriers. This is consistent with the resistance divider ratio for ROMK discussed above if the outer two wells and three barriers, which should cover two thirds of the electric field across the pore, correspond to the outer resistor. To reduce the number of free parameters, the depths of outer and middle wells were set to be equal (Fig. 9 A). The theoretical I-V curve is based on an energy profile that accurately, but not uniquely, simulated the experimental data. Next, we fixed the parameters for K^+ and changed the energy profile parameters for NH_4^+ to fit the I-V curve for the bi-ionic condition of NH_4^+ outside and K^+ inside the cell (Fig. 9 B). Again, the depths of outer and middle wells for the NH_4^+ energy profile

were set to be equal. The best-fit energy profile suggests that NH_4^+ has significantly lower affinities than does K^+ for the binding sites within the pore, as indicated by the shallower energy wells for NH_4^+ than for K^+ in the diagram. The higher affinity for K^+, particularly of the energy well closest to the cytoplasmic side, mainly accounts for the higher K^+ permeability since this site will be predominantly occupied by K^+ at membrane potentials positive to −60 mV (Fig. 7 B), preventing NH_4^+ flow through the channel. On the other hand, the hyperpolarized potentials associated with inward current would prevent occupancy of the channel by K^+ and favor occupancy by NH_4^+. Under these conditions, the inward NH_4^+ conductance is large because the middle energy barriers to NH_4^+ movement are lower than those to K^+, increasing its mobility within the pore. We conclude that simple energy barrier models can explain the unusual selectivity pattern of K^+ and NH_4^+.

Summary

In summary, the differences in K^+ conductance among ROMK, IRK, and various chimeras can be roughly explained by a model with two resistors in series, composed of the extracellular region and the COOH terminus. The NH_4^+ and Rb^+ selectivity differences between

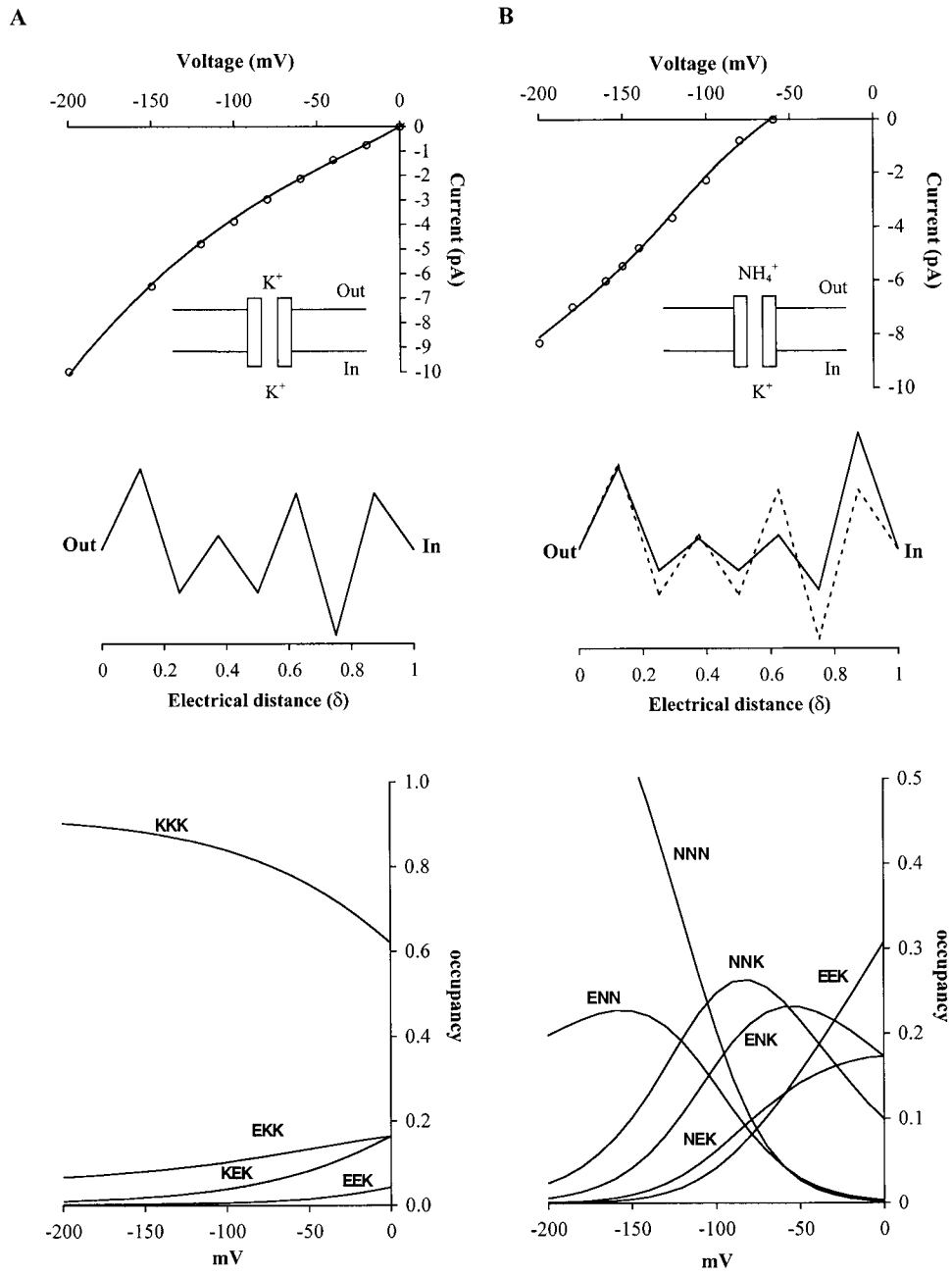

Figure 9.

ROMK2 and IRK1 depend on the extracellular loop region, and specifically on the amino acid at the 3P position. On the other hand, the cytoplasmic termini seem to be at least partly the locus of Tl^+ selectivity. The unusual selectivity pattern of K^+ and NH_4^+ can be explained by a simple energy barrier model.

This work was supported by National Institutes of Health grants DK27847 (L.G. Palmer) and DK46950 (H. Sackin).

Henry Lester served as guest editor.

Submitted: 7 December 1999
Revised: 31 January 2000
Accepted: 7 February 2000

REFERENCES

Abrams, C.J., N.W. Davies, P.A. Shelton, and P.R. Stanfield. 1996. The role of a single aspartate residue in ionic selectivity and block of a murine inward rectifier K^+ channel Kir2.1. *J. Physiol.* 493:643–649.

Armstrong, C.M. 1969. Inactivation of the potassium conductance and related phenomena caused by quaternary ammonium ion injection in squid axons. *J. Gen. Physiol.* 54:553–575.

Armstrong, C.M. 1971. Interaction of tetraethylammonium ion derivatives with the potassium channels of giant axons. *J. Gen. Physiol.* 58:413–437.

Ashcroft, F.M., and P.R. Stanfield. 1983. The influence of the permeant ions thallous and potassium on inward rectification in frog skeletal muscle. *J. Physiol.* 343:407–428.

Begenisich, T.B., and M.D. Cahalan. 1980. Sodium channel permeation in squid axons. I: Reversal potential experiments. *J. Physiol.* 307:217–242.

Bezanilla, F., and C.M. Armstrong. 1972. Negative conductance caused by entry of sodium and cesium ions into the potassium channels of squid axons. *J. Gen. Physiol.* 60:588–608.

Blatz, A.L., and K.L. Magleby. 1984. Ion conductance and selectivity of single calcium-activated potassium channels in cultured rat muscle. *J. Gen. Physiol.* 84:1–23.

Case, D.A., and M. Karplus. 1979. Dynamics of ligand binding to heme proteins. *J. Mol. Biol.* 132:343–368.

Chepilko, S., H. Zhou, H. Sackin, and L.G. Palmer. 1995. Permeation and gating properties of a cloned renal K^+ channel. *Am. J. Physiol. Cell Physiol.* 268:C389–C401.

Choe, H. 1999. Structure–function relationships of inward-rectifier K^+ channels. Ph.D. Thesis. Weill Graduate School of Medical Sciences of Cornell University, New York, NY.

Choe, H., L.G. Palmer, and H. Sackin. 1999. Structural determinants of gating in inward-rectifier K^+ channels. *Biophys. J.* 76: 1988–2003.

Choe, H., H. Sackin, and L.G. Palmer. 1998. Permeation and gating of an inwardly rectifying potassium channel. Evidence for a variable energy well. *J. Gen. Physiol.* 112:433–446.

Doyle, D.A., J.M. Cabral, R.A. Pfuetzner, A. Kuo, J.M. Gulbis, S.L. Cohen, B.T. Chait, and R. MacKinnon. 1998. The structure of the potassium channel: molecular basis of K^+ conduction and selectivity. *Science.* 280:69–77.

Eisenman, G., R. Latorre, and C. Miller. 1986. Multi-ion conduction and selectivity in the high-conductance Ca^{++}-activated K^+ channel from skeletal muscle. *Biophys. J.* 50:1025–1034.

Elber, R., and M. Karplus. 1987. Multiple conformational states of proteins: a molecular dynamics analysis of myoglobin. *Science.* 235:318–321.

Fakler, B., U. Brandle, C. Bond, E. Glowatzki, C. Konig, J.P. Adelman, H.P. Zenner, and J.P. Ruppersberg. 1994. A structural determinant of differential sensitivity of cloned inward rectifier K^+ channels to intracellular spermine. *FEBS Lett.* 356:199–203.

Glowatzki, E., G. Fakler, U. Brandle, U. Rexhausen, H.P. Zenner, J.P. Ruppersberg, and B. Fakler. 1995. Subunit-dependent assembly of inward-rectifier K^+ channels. *Proc. R. Soc. Lond. B Biol. Sci.* 261:251–261.

Hagiwara, S., and K. Takahashi. 1974. The anomalous rectification and cation selectivity of the membrane of a starfish egg cell. *J. Membr. Biol.* 18:61–80.

Harris, R.E., H.P. Larsson, and E.Y. Isacoff. 1998. A permanent ion binding site located between two gates of the *Shaker* K^+ channel.

Figure 9. Three-site four-barrier kinetic model. (A, top) Single channel I-V plots for K^+ current through ROMK2 channel (110 mM KCl in the pipette in the cell-attached mode). The line is the best-fit to the data using the three-site four-barrier kinetic model, which gives rise to the following rate constants (s^{-1}) (Scheme I). V1, V2, and V3 represent the first, second, and third energy wells from the outside.

$$\text{Out} \underset{1.7\times10^{8}}{\overset{6.6\times10^{9}}{\rightleftharpoons}} \text{V1} \underset{5.1\times10^{10}}{\overset{5.1\times10^{10}}{\rightleftharpoons}} \text{V2} \underset{3.7\times10^{7}}{\overset{1.4\times10^{9}}{\rightleftharpoons}} \text{V3} \underset{5.3\times10^{10}}{\overset{3.8\times10^{7}}{\rightleftharpoons}} \text{In} \qquad \text{(SCHEME I)}$$

(Middle) The energy profile for K^+ ion along the pore of ROMK2 at 0 mV. The shape of the energy profiles was constructed from the kinetic model. (Bottom) Occupancy plot of each state as a function of voltage for the K^+ ion in the pore of ROMK2. The symbol KKK indicates the state that all three energy wells are occupied by K^+, and the symbol EKK indicates the state that the second and the third energy wells from outside are occupied by K^+. The pore is occupied by at least two K^+ ions most of the time. The occupancies of the two states, KKE and EEE, are very small and not shown. (B, top) Single channel I-V plots of ROMK2 with NH_4^+ (110 mM) outside and K^+ (110 mM) inside the cell. The line is the best-fit to the data using the three-site four-barrier kinetic model with the same rate constants as in A for K^+. The fitting procedure produced the following kinetic rates for NH_4^+ (Scheme II).

$$\text{Out} \underset{1.4\times10^{9}}{\overset{8.3\times10^{9}}{\rightleftharpoons}} \text{V1} \underset{4.6\times10^{11}}{\overset{4.6\times10^{11}}{\rightleftharpoons}} \text{V2} \underset{7.7\times10^{10}}{\overset{3.6\times10^{11}}{\rightleftharpoons}} \text{V3} \underset{5.2\times10^{8}}{\overset{2.0\times10^{7}}{\rightleftharpoons}} \text{In} \qquad \text{(SCHEME II)}$$

(Middle) The ion energy profile (solid) for NH_4^+ ion along the pore of ROMK2 at 0 mV, obtained from the kinetic model for NH_4^+. The dotted energy profile is for K^+ in A for comparison. The energy wells for NH_4^+ are shallower than those for K^+, suggesting weaker affinity for NH_4^+. (Bottom) Occupancy plot of each state as a function of voltage in the pore of ROMK2 with NH_4^+ outside and K^+ inside. The symbol NNN means that all three sites are occupied by NH_4^+, and the symbol NEK means that the outer and inner wells are occupied by NH_4^+ and K^+, respectively. States with small occupancies are not shown for clarity.

Biophys J. 74:1808–1820.

Hasinoff, B.B. 1977. The diffusion-controlled reaction kinetics of the binding of CO and O_2 to myoglobin in glycerol-water mixtures of high viscosity. *Arch. Biochem. Biophys.* 183:176–188.

Heginbotham, L., Z. Lu, T. Abramson, and R. MacKinnon. 1994. Mutations in the K^+ channel signature sequence. *Biophys. J.* 66: 1061–1067.

Heginbotham, L., and R. MacKinnon. 1993. Conduction properties of the cloned *Shaker* K^+ channel. *Biophys. J.* 65:2089–2096.

Hille, B. 1973. Potassium channels in myelinated nerve. Selective permeability to small cations. *J. Gen. Physiol.* 61:669–686.

Hille, B. 1992. Ionic channels of excitable membranes. 2nd edition. Sinauer Associates, Inc., Sunderland, MA. 362–389.

Hol, W.G. 1985. The role of the alpha-helix dipole in protein function and structure. *Prog. Biophys. Mol. Biol.* 45:149–195.

Horie, M., and H. Irisawa. 1989. Dual effects of intracellular magnesium on muscarinic potassium channel current in single guinea-pig atrial cells. *J. Physiol.* 408:313–332.

Horie, M., H. Irisawa, and A. Noma. 1987. Voltage-dependent magnesium block of adenosine-triphosphate–sensitive potassium channel in guinea-pig ventricular cells. *J. Physiol.* 387:251–272.

Jan, L.Y., and Y.N. Jan. 1997. Cloned potassium channels from eukaryotes and prokaryotes. *Annu. Rev. Neurosci.* 20:91–123.

Kubo, Y., T.J. Baldwin, Y.N. Jan, and L.Y. Jan. 1993. Primary structure and functional expression of a mouse inward rectifier potassium channel. *Nature.* 362:127–133.

Latorre, R., and C. Miller. 1983. Conduction and selectivity in potassium channels. *J. Membr. Biol.* 71:11–30.

Lopatin, A.N., E.N. Makhina, and C.G. Nichols. 1994. Potassium channel block by cytoplasmic polyamines as the mechanism of intrinsic rectification. *Nature.* 372:366–369.

Lopatin, A.N., E.N. Makhina, and C.G. Nichols. 1995. The mechanism of inward rectification of potassium channels: "long-pore plugging" by cytoplasmic polyamines. *J. Gen. Physiol.* 106:923–955.

Lopatin, A.N., and C.G. Nichols. 1996. [K^+] dependence of polyamine-induced rectification in inward rectifier potassium channels (IRK1, Kir2.1). *J. Gen. Physiol.* 108:105–113.

Lopez, G.A., Y.N. Jan, and L.Y. Jan. 1994. Evidence that the S6 segment of the Shaker voltage-gated K^+ channel comprises part of the pore. *Nature.* 367:179–182.

Lu, Z., and R. MacKinnon. 1994. Electrostatic tuning of Mg^{2+} affinity in an inward-rectifier K^+ channel. *Nature.* 371:243–246.

Matsuda, H. 1988. Open-state substructure of inwardly rectifying potassium channels revealed by magnesium block in guinea-pig heart cells. *J. Physiol.* 397:237–258.

Mullins, L.J. 1959. The penetration of some cations into muscle. *J. Gen. Physiol.* 42:817–829.

Nichols, C.G., K. Ho, and S. Hebert. 1994. Mg(2+)-dependent inward rectification of ROMK1 potassium channels expressed in *Xenopus* oocytes. *J. Physiol.* 476:399–409.

Nichols, C.G., and A.N. Lopatin. 1997. Inward rectifier potassium channels. *Annu. Rev. Physiol.* 59:171–191.

Pearson, W.L., and C.G. Nichols. 1998. Block of the Kir2.1 channel pore by alkylamine analogues of endogenous polyamines. *J. Gen. Physiol.* 112:351–363.

Perez-Cornejo, P., and T. Begenisich. 1994. The multi-ion nature of the pore in *Shaker* K^+ channels. *Biophys. J.* 66:1929–1938.

Perutz, M.F., and F.S. Mathews. 1966. An x-ray study of azide methaemoglobin. *J. Mol. Biol.* 21:199–202.

Reuter, H., and C.F. Stevens. 1980. Ion conductance and ion selectivity of potassium channels in snail neurones. *J. Membr. Biol.* 57: 103–118.

Reuveny, E., Y.N. Jan, and L.Y. Jan. 1996. Contributions of a negatively charged residue in the hydrophobic domain of the IRK1 inwardly rectifying K^+ channel to K(+)-selective permeation. *Biophys. J.* 70:754–761.

Sabirov, R.Z., T. Tominaga, A. Miwa, Y. Okada, and S. Oiki. 1997. A conserved arginine residue in the pore region of an inward rectifier K channel (IRK1) as an external barrier for cationic blockers. *J. Gen. Physiol.* 110:665–677.

Shapiro, M.S., and T.E. DeCoursey. 1991. Selectivity and gating of the type L potassium channel in mouse lymphocytes. *J. Gen. Physiol.* 97:1227–1250.

Sigworth, F.J., and S.M. Sine. 1987. Data transformations for improved display and fitting of single-channel dwell time histograms. *Biophys. J.* 52:1047–1054.

Spassova, M., and Z. Lu. 1998. Coupled ion movement underlies rectification in an inward-rectifier K^+ channel. *J. Gen. Physiol.* 112:211–221.

Spruce, A.E., N.B. Standen, and P.R. Stanfield. 1987. Studies of the unitary properties of adenosine-5′-triphosphate–regulated potassium channels of frog skeletal muscle. *J. Physiol.* 382:213–236.

Standen, N.B., and P.R. Stanfield. 1980. Rubidium block and rubidium permeability of the inward rectifier of frog skeletal muscle fibres. *J. Physiol.* 304:415–435.

Stanfield, P.R., N.W. Davies, P.A. Shelton, M.J. Sutcliffe, I.A. Khan, W.J. Brammar, and E.C. Conley. 1994. A single aspartate residue is involved in both intrinsic gating and blockage by Mg^{2+} of the inward rectifier, IRK1. *J. Physiol.* 478:1–6.

Taglialatela, M., E. Ficker, B.A. Wible, and A.M. Brown. 1995. C-terminus determinants for Mg^{2+} and polyamine block of the inward rectifier K^+ channel IRK1. *EMBO (Eur. Mol. Biol. Organ.) J.* 14: 5532–5541.

Taglialatela, M., B.A. Wible, R. Caporaso, and A.M. Brown. 1994. Specification of pore properties by the carboxyl terminus of inwardly rectifying K^+ channels. *Science.* 264:844–847.

Taylor, P.S. 1987. Selectivity and patch measurements of A-current channels in Helix aspersa neurones. *J. Physiol.* 388:437–447.

Welling, P.A. 1997. Primary structure and functional expression of a cortical collecting duct Kir channel. *Am. J. Physiol. Renal Physiol.* 273:F825–F836.

Wible, B.A., M. Taglialatela, E. Ficker, and A.M. Brown. 1994. Gating of inwardly rectifying K^+ channels localized to a single negatively charged residue. *Nature.* 371:246–249.

Yang, J., Y.N. Jan, and L.Y. Jan. 1995a. Control of rectification and permeation by residues in two distinct domains in an inward rectifier K^+ channel. *Neuron.* 14:1047–1054.

Yang, J., Y.N. Jan, and L.Y. Jan. 1995b. Determination of the subunit stoichiometry of an inwardly rectifying potassium channel. *Neuron.* 15:1441–1447.

Yool, A.J., and T.L. Schwarz. 1991. Alteration of ionic selectivity of a K^+ channel by mutation of the H5 region. *Nature.* 349:700–704.

Yool, A.J., and T.L. Schwarz. 1996. Anomalous mole fraction effect induced by mutation of the H5 pore region in the *Shaker* K^+ channel. *Biophys. J.* 71:2467–2472.

Zhou, H., S. Chepilko, W. Schutt, H. Choe, L.G. Palmer, and H. Sackin. 1996. Mutations in the pore region of ROMK enhance Ba^{2+} block. *Am. J. Physiol. Cell Physiol.* 271:C1949–C1956.

Zhou, H., S.S. Tate, and L.G. Palmer. 1994. Primary structure and functional properties of an epithelial K channel. *Am. J. Physiol. Cell Physiol.* 266:C809–C824.